Local Iron Loss Identification by Thermal Measurements on an Outer-Rotor Permanent Magnet Synchronous Machine

Andreas Krings, Shafigh Nategh, Oskar Wallmark, and Juliette Soulard

Department of Electrical Energy Conversion (E2C)
KTH Royal Institute of Technology, Stockholm, Sweden

***Abstract*—This paper presents the experimental determination of iron losses in an outer-rotor permanent magnet synchronous machine (PMSM) by using an inverse thermal model (ITM) in connection with transient thermal measurements. First, the theory and assumptions lying behind the method are presented. Afterwards, 3D finite element method (FEM) based simulations are used to determine the flux density distribution and iron losses in the magnetic steel parts of the investigated machine. Thermal measurements are conducted to determine local iron losses in the stator tooth tips using the ITM. Finally, measurement and FEM simulation results are compared.**

***Index Terms*—AC machines, iron losses, loss measurement, permanent magnet machines, thermal measurement.**

I. Introduction

Accurate prediction of iron losses are one of the key points when it comes to performance improvements of electrical machines. But there is still a large discrepancy between simulation and measurement results. So called "build factors" [1] or "loss correction factors" [2] in the range of $1.1-2$ are still commonly used to match simulations with corresponding experimental results. However, it is not possible to determine iron losses directly [3]. The IEC standard 60034-2-1 [4] defines the iron losses by subtracting mechanical and copper losses from the total input power of the machine. Another way to determine iron losses is by investigating the magnetic flux density and magnetic field intensity in the iron parts of the machine, measured for example with search coils and Gauss meters. However, this method is difficult to apply to complex machine geometries and heavily depending on the chosen iron loss model [5]. A physical measurable quantity related to losses is the temperature [6] [7]. It is not just possible to determine temperature distributions from generated losses but also to determine losses from temperature distribution and changes. This paper describes an indirect experimental method to determine iron losses from transient thermal measurements by using an inverse thermal model (ITM).

A thermal loss investigation on a $5.5\,\mathrm{kW}$ induction motor equipped with 100 thermal sensors in the stator and squirrel cage rotor is presented in [8]. In this study, the losses are determined by inverting and over-determining the matrix of the thermal lumped-parameter machine model at steady-state. A transient thermal loss investigation for determining losses from temperature changes by applying an ITM is presented in [9]. The method is applied on a large water-wheel synchronous generator ($80\,\mathrm{MW}$) equipped with 300 thermal sensors to determine the local iron losses at different locations in the stator core of the machine. Both approaches have the drawback that a large amount of sensors is used. Such investigations can only be realized with prototypes where the sensors are installed during the manufacturing process but not with finally assembled machines.

In this presented work the transient temperature investigation approach was chosen to experimentally determine the iron losses in an already assembled $785\,\mathrm{W}$ outer-rotor permanent magnet synchronous machine (PMSM). The thermal sensors are installed on the stator teeth of the machine to investigate the local iron losses. The losses are calculated with the ITM method and compared to finite element method (FEM) based simulations.

First, the theory of the ITM is described in Section II and the investigated outer-rotor PMSM is presented in Section III. Section V introduces the thermal measurements and determined iron losses, followed by the investigated FEM simulations in Section IV. A comparison between the measurement and simulation results is presented in Section VI. Section VII provides the conclusions of this work.

II. Inverse Thermal Modeling

Assuming constant material properties (e.g. isotropic material and the thermal conductivity and specific heat capacitance are not depending on the temperature), the general heat diffusion equation (often called heat equation) can be expressed as in [10], [11]

$$\frac{\mathrm{d}\vartheta}{\mathrm{d}t} = a\,\nabla^2\vartheta + \frac{p_{\mathrm{gen}}}{c_{\mathrm{th}}\,\gamma} \tag{1}$$

with the thermal diffusivity

$$a = \frac{\sigma_{\mathrm{th}}}{c_{\mathrm{th}}\,\gamma}. \tag{2}$$

Here, c_{th} is the specific thermal capacity in J/(kg K), γ the material density in kg/m^3, σ_{th} the thermal conductivity in W/(K m), p_{gen} the power density in W/m^3, and ϑ the temperature in K.

At steady state, equation (1) states that the power generation or absorption inside an investigated volume is equal to its local temperature distribution. It is used as the initial point of the ITM. The measurement is started from a steady-state condition with constant distributed temperature in a volume which is a small part of the investigated device. Then, the

A. Krings, S. Nategh, O. Wallmark, and J. Soulard are with the Department of Electrical Energy Conversion (E2C), Royal Institute of Technology (KTH), SE-10044 Stockholm, Sweden (e-mail: andreas.krings@ee.kth.se, juliette.soulard@ee.kth.se).

power generation inside the investigated volume is changed instantly and (1) is changed to (3)

$$\left(\frac{\mathrm{d}\vartheta}{\mathrm{d}t}\right)_{t\to 0^+} = a\nabla^2\vartheta + \frac{p_{\mathrm{gen}}}{c_{\mathrm{th}}\gamma}. \tag{3}$$

It is now assumed that the heat transfer inside the investigated volume is negligible during the first instant after the power change. This means that $a\,\nabla^2\,\vartheta \ll \frac{p_{\mathrm{gen}}}{c_{\mathrm{th}}\,\gamma}$ is fulfilled. In this case, the diffusion term on the right hand side of (3) can be neglected and (3) simplifies to

$$\left(\frac{\mathrm{d}\vartheta}{\mathrm{d}t}\right)_{t\to 0^+} = \frac{p_{\mathrm{gen}}}{c_{\mathrm{th}}\gamma}. \tag{4}$$

Reordering (4) yields

$$p_{\mathrm{gen}} = c_{\mathrm{th}}\gamma\left(\frac{\mathrm{d}\vartheta}{\mathrm{d}t}\right)_{t\to 0^+} \tag{5}$$

which is referred to as the inverse thermal model (ITM) in the following.

The ITM allows the determination of losses generated in an arbitrary point of a volume by measuring the change of temperature during the first instant of time after a thermal equilibrium steady-state condition. Thus, the change in slope of the temperature immediately after a change of power can be used to determine the losses in the point of interest. A required assumption is that all external conditions, such as cooling, remain unchanged, at least during the initial phase preceding the change in losses. Furthermore, the heat transfer inside the volume must also be negligible during the investigation time.

III. The Investigated Machine

The investigated outer-rotor PMSM shown in Fig. 1 has a concentrated double-layer winding with 28 poles and 24 slots. Ferrite magnets are mounted on the inside surface of the outer rotor. The technical data of the motor are reported in Table I. The stator core is built from M800-50A lamination sheets and each tooth is wound with 181 turns.

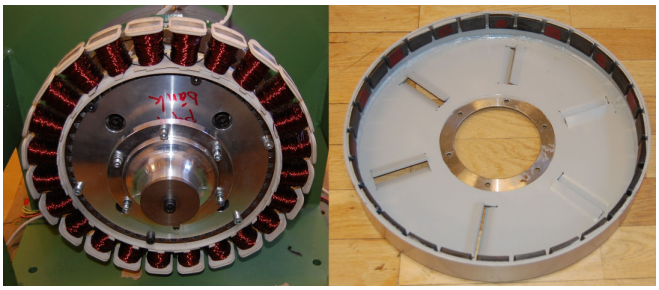

Fig. 1. Stator and rotor of the investigated outer-rotor PMSM.

TABLE I
Motor data

Rated torque:	30 Nm
Rated speed:	200 rpm
Maximum speed:	1200 rpm
Maximum power:	785 W
Rated current (RMS):	3.4 A
Measured d-axis inductance L_d:	0.96 mH
Rotor outer diameter [mm]:	404
Stator outer diameter [mm]:	374
Airgap length [mm]:	1
Axial length stator [mm]:	20
Active axial length rotor [mm]:	25

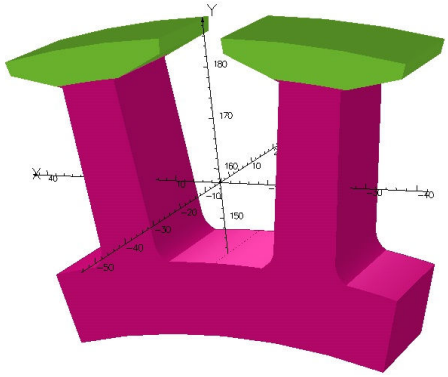

Fig. 2. Stator tooth tips (green) and stator tooth yoke (violet).

IV. FEM Simulations

The machine is simulated at no-load condition (i.e. there is no current flowing in the winding) at 300 rpm, 500 rpm and 700 rpm to determine the expected no-load iron losses in the stator core, with a special focus on the stator tooth tips. All simulations are performed with a 3D FEM solver to take into account the different active lengths of the stator core (20 mm) and the permanent magnets in the rotor (25 mm). The stacking factor is set to 0.98 and an anisotropic conductivity of 4.35×10^6 S/m from [12] is used in the directions inside the lamination plane. The density of the magnetic material is 7800 kg/m^3. The magnetic material parameters for the stator core are applied as a non-linear initial BH-curve based on the values from M800-50A electrical steel sheets [12]. The stator teeth are separated into two volumes, namely the stator tooth tips and the stator tooth yoke, as shown in Fig. 2. This allows a more clear iron loss separation and a better comparison to the measured iron losses in the stator tooth tips.

The iron losses in the stator tooth tips are determined by separating the losses into hysteresis losses, eddy current losses and excess losses, as given in (6) [13].

$$p_{\mathrm{Fe}} = C_{\mathrm{hyst}}\, f\, \hat{B}^2 + C_{\mathrm{EC}}\, f^2\, \hat{B}^2 + C_{\mathrm{exc}}\, f^{1.5}\, \hat{B}^{1.5} \tag{6}$$

Here, f is the frequency, C_{hyst} is the hysteresis loss coefficient, C_{EC} the eddy current loss coefficient, and C_{exc} is the excess loss coefficient. The coefficients are determined by surface fitting the iron loss data from [14] with (6). The determined loss coefficients are 306, 2.18, and $3.4e-5$, for C_{hyst}, C_{EC}, and C_{exc}, respectively. Eq. (6) is used in the FEM post-processing to determine the iron loss density in each element from the fundamental flux density and the flux density harmonics up to the 9th order. The average iron loss density in the tooth tips is 5.15 W/kg, 10.64 W/kg and 19.57 W/kg for 300 rpm, 500 rpm and 700 rpm, respectively. Fig. 3 shows the current vectors and the iron loss density in the stator for an arbitrary rotor position at 700 rpm.

V. Thermal Measurements

The thermal measurement setup of the outer-rotor PMSM is shown in Fig. 4. The temperature of the machine stator core is measured by three PT100 sensors and a thermal infrared camera (Flir SC655). Two PT100 thermal sensors are mounted on one stator tooth. The first one (sensor 1) is located on the front side of the stator tooth tip behind the plastic insulation shield of the winding, and the second one

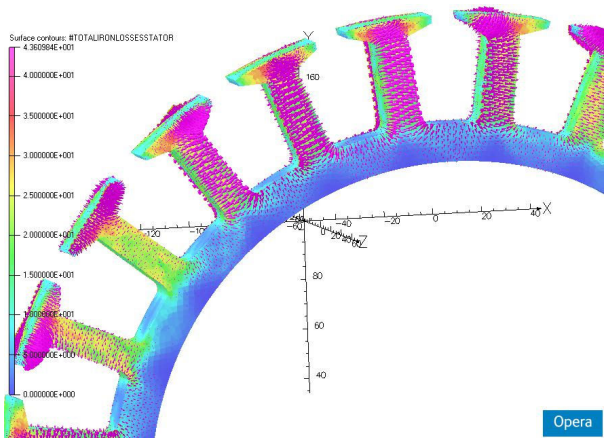

Fig. 3. Iron loss density (surface contour in W/kg) and current density vectors at no-load, 700 rpm.

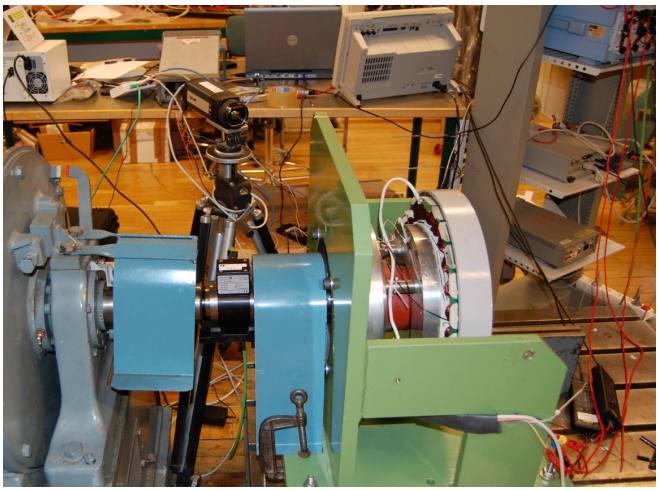

Fig. 4. Thermal measurement setup of the investigated outer-rotor PMSM.

(sensor 2) is installed on top of the coil lower front side on the same stator tooth. Both sensors are shown in Fig. 5. The third sensor (sensor 3) is mounted on the stator yoke back side inside the outer rotor. To reduce the cooling capabilities and minimize the turbulent air flow in the machine, the axial cooling ducts on the back side of the rotor, visible on the right picture in Fig. 1, are covered with transparent tape.

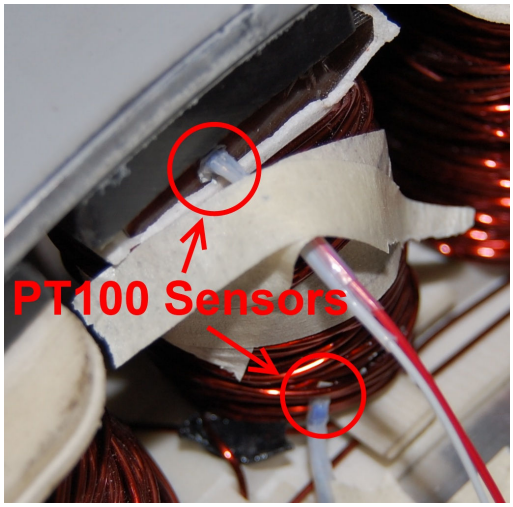

Fig. 5. PT100 temperature sensors mounted on the front side of the stator tooth tip and on the winding coil.

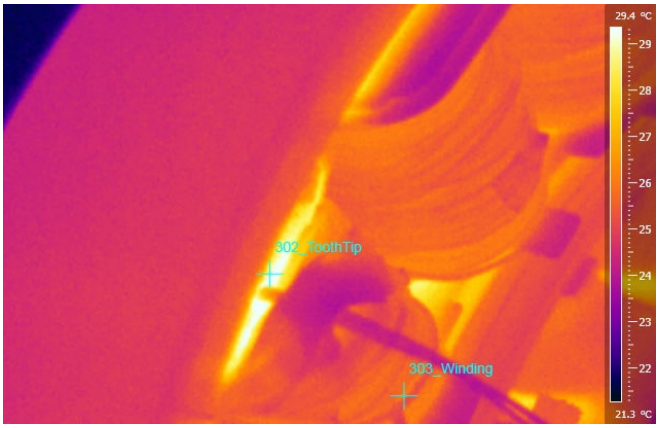

Fig. 6. Thermal image of the stator coils and mounted PT100 sensors at a no-load test with 700 rpm.

For the tests the investigated outer-rotor PMSM is driven by a synchronous machine at constant speed with open terminals so that there is no current flowing in the windings. It is assumed that all measured losses and all of the corresponding temperature increases in the stator core are caused by iron losses (friction and windage losses can be neglected since they do not heat up the stator core during the investigation time). The tests are performed at 300 rpm, 500 rpm and 700 rpm at constant room temperature (22 °C). The temperature sensors are sampled every third second and the thermal infrared camera records the temperature at a sampling rate of 10 Hz. Fig. 6 shows a thermal picture of the stator teeth and coils at no-load test with 700 rpm.

The measurement results of the PT100 temperature sensors 1 and 3 are shown in Fig. 7. Sensor 1 (mounted on the stator tooth tip front side) has the largest temperature raise due to iron losses in the tooth tips induced from the flux of the permanent magnets. With increasing speed of the rotor, the frequency of the flux in the stator core increases and so do the iron losses. Sensor 3 (mounted on the stator yoke back side) has a smaller temperature increase due to lower iron losses in the stator yoke and a turbulent air flow around the sensor created by the turning rotor core. This air flow might also be the cause for the delayed temperature rise compared to sensor 1. The temperature increase of the winding surface (sensor 2) is marginal in the no-load case and just caused by the heat transfer from the stator teeth and tooth tips through the copper coil winding.

For the ITM method, the boundary conditions are assumed to be constant. This means that the cooling and air flow in the first instant of change after the steady-state must not influence the sensors. This is only valid for sensor 1, since this sensor is mounted behind the winding shield. It is not influenced by the airflow from the rotor. Sensor 3 is directly located in the turbulent airflow inside the outer rotor and thus heavily influenced by the air cooling. At the no-load test condition, sensor 2 is not directly located at a loss source and therefore also neglected in the following investigations.

To determine the local iron loss density in the tooth tips, the ITM method is only applied to the thermal measurement results of sensor 1. Fig. 8 shows the initial temperature increase curves of sensor 1 for the operating speeds of 300 rpm, 500 rpm and 700 rpm. The difficulty is that the losses have to be obtained from the slope of temperature change in the first instant of time after the change from the

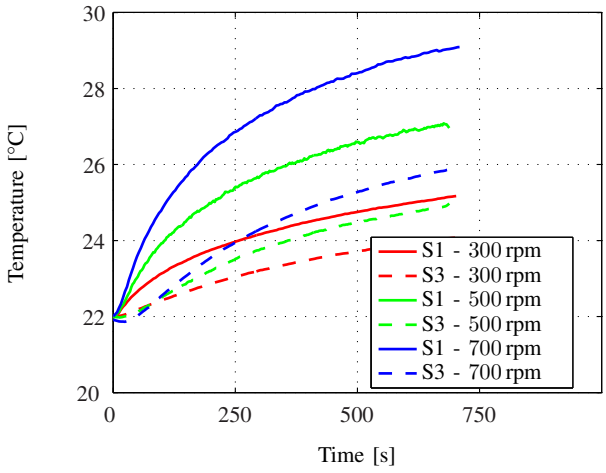

Fig. 7. Temperature rises of Sensor 1 (S1) and Sensor 3 (S3) at no-load condition for 300 rpm, 500 rpm and 700 rpm.

steady-state condition, thus before any heat conduction and diffusion takes place [9] [15].

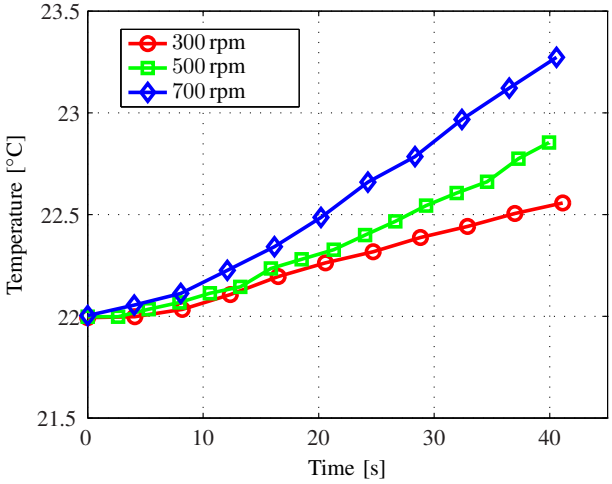

Fig. 8. Initial temperature rise of sensor 1 for 300 rpm, 500 rpm and 700 rpm.

The largest initial temperature slopes in figure 8 are determined to 15.45 mK/s, 21.21 mK/s and 36.02 mK/s. Using (5) yields the losses 9.31 W/kg, 12.78 W/kg and 21.7 W/kg. This increase in loss with a polynomial growth is expected since the eddy current part of the iron losses is increasing with the square of the frequency.

VI. Comparison of Simulation and Measurements

The FEM simulation and measurement results of the iron loss density in the stator tooth tips at no-load are shown in Fig. 9. The measured loss density results determined by the ITM method show a strong non-linear increase with frequency for the specific iron losses. The iron losses determined from the FEM simulation and (6) also show a non-linear increase but much smoother, as can be seen from the blue 'X' in figure 9. The agreement between the measurements and FEM simulations is quite good, especially for the operating points at 500 rpm and 700 rpm. The larger discrepancy at 300 rpm is probably due to a inaccurate determination of the temperature slope. Temperature increases

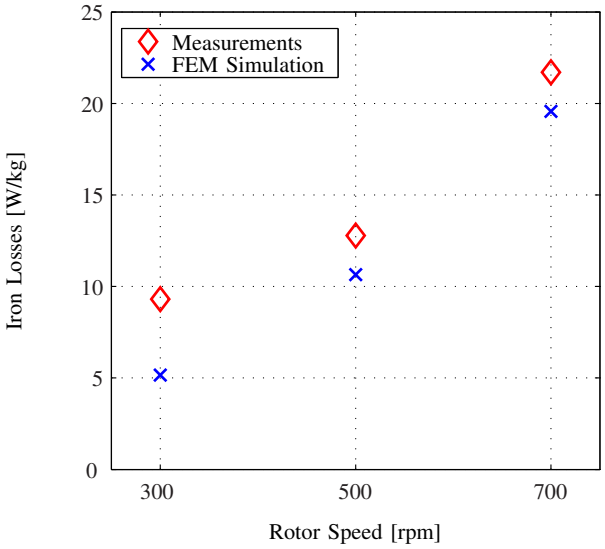

Fig. 9. Iron loss density in the stator tooth tips determined by FEM calculations and thermal measurements for 300 rpm, 500 rpm and 700 rpm.

of less than 15 mK/s are difficult to determine exactly with standard PT100 sensors and lab equipment.

In summary, the presented results from the ITM method differ to some extent from the FEM results, especially for small frequencies and thus low losses in the machine. The compliance of the measurement and simulation results becomes much closer at higher frequencies and thus larger losses. But even if the maximum measurement values are used at higher frequencies, they are still smaller than the FEM simulation results. This will introduce loss correction factors in the range of $1.1-1.8$ for further simulations, as mentioned in the introduction of this paper.

VII. Conclusions

The inverse thermal model (ITM) was applied to the stator tooth tips of an outer-rotor PMSM for investigating local iron losses. The investigated machine was operated at no-load condition for three different speeds. Satisfactory results with some discrepancies between the measurements and FEM simulations were achieved. Although the investigated machine has a low power density and is not specially suited for iron loss investigations, it was shown that the ITM has potential for local iron loss investigations of complex machine geometries. An important requirement is the accessibility of the interesting locations by thermal sensors, which should be taken into account during the manufacturing process for enclosed machines. The most challenging and complicated part of the ITM is the determination of the initial temperature rise starting point for the correct calculation of the temperature slope and thus the associated losses. Temperature slopes in the range of several mK/s must be accurately determined during the experiment.

VIII. Acknowledgment

The authors would like to thank gratefully Thord Nilson from Danaher Motion, Stockholm, Sweden, and Dr. Florence Meier from Bombardier Transportation, Västerås, Sweden, for invaluable discussions and test data. Furthermore, thanks are given to Nikhil Sawant from Cobham Technical Services, Vector Fields Software, for supporting the FEM simulations.

REFERENCES

[1] Oka, M. Kawano, K. Shimada, T. Kai, and M. Enokizono, "Evaluation of the magnetic properties of the rotating machines for the building factor clarification," *Przeglad Elektrotechniczny (Electrical Review)*, vol. 87, no. 9B, pp. 43–46, 2011.

[2] W. Roshen, "Iron loss model for permanent-magnet synchronous motors," *IEEE Transactions on Magnetics*, vol. 43, no. 8, pp. 3428–3434, 2007.

[3] A. Krings, S. Nategh, A. Stening, H. Grop, O. Wallmark, and J. Soulard, "Measurement and modeling of iron losses in electrical machines," in *5th International Conference Magnetism and Metallurgy WMM'12*, Gent, Belgium, 2012, pp. 101–119.

[4] "Standard methods for determining losses and efficiency from tests (excluding machines for traction vehicles)," International Standard IEC 60034-2-1:2007.

[5] A. Krings and J. Soulard, "Overview and comparison of iron loss models for electrical machines," *Journal of Electrical Engineering*, vol. 10, no. 3, pp. 162–169, 2010.

[6] D. Staton, A. Boglietti, and A. Cavagnino, "Solving the more difficult aspects of electric motor thermal analysis in small and medium size industrial induction motors," *IEEE Transactions on Energy Conversion*, vol. 20, no. 3, pp. 620–628, 2005.

[7] S. Nategh, O. Wallmark, M. Leksell, and S. Zhao, "Thermal analysis of a PMaSRM using partial FEA and lumped parameter modeling," *IEEE Transactions on Energy Conversion*, vol. 27, no. 2, pp. 477 –488, 2012.

[8] J. Trigeol, M. Girault, P. Lagonotte, Y. Bertin, and D. Petit, "Estimation of the heat losses in an electrical machine using an inverse method," in *16th International Conference on Electrical Machines (ICEM), 2004*, Cracow, Poland, 2004, p. 5.

[9] A. Gilbert, "A method of measuring loss distribution in electrical machines," *Proceedings of the IEE - Part A: Power Engineering*, vol. 108, no. 39, pp. 239–244, 1961.

[10] H. D. Baehr and K. Stephan, *Heat and Mass Transfer*, 2nd ed. Springer, 2006.

[11] F. P. Incropera, D. P. DeWitt, T. L. Bergman, and A. S. Lavine, *Fundamentals of Heat and Mass Transfer*, 6th ed. Wiley, 2006.

[12] "Technical datasheet M800-50A - Cogent Surahammars Bruks AB," 2008.

[13] F. Fiorillo and A. Novikov, "An improved approach to power losses in magnetic laminations under nonsinusoidal induction waveform," *IEEE Transactions on Magnetics*, vol. 26, no. 5, pp. 2904–2910, 1990.

[14] "Technical datasheet PowerCore M800-50A - ThyssenKrupp Steel Europe," 2009.

[15] J. Trigeol, "Identification des pertes d'une machine électrique par une approche thermique et à l'aide d'une technique inverse," PhD Thesis, Université de Poitiers, 2004.